European Review for Medical and Pharmacological Sciences 2022; 26: (3 Suppl): 11-20

Tissue reconstruction of abdominal wall with butyric acid-based nets: preliminary *in vitro* test using tissue engineering strategies

I. ZANOLLA[1], E. TIENGO[1], F. ZANOTTI[1], M. TRENTINI[1], C. MORTELLARO[2], A.G. LUCCHINA[2], D. LICASTRO[3], S. DAL MONEGO[3], G. SOLIANI[4], B. ZAVAN[1]

[1]Department of Translational Medicine, University of Ferrara, Ferrara, Italy
[2]Regenerative Medicine and Tissue Engineering, Saint Camillus International University of Health and Medical Science, Rome Italy
[3]AREA Science Park, Padriciano, Trieste, Italy
[4]Department of Surgery, S. Anna University Hospital and University of Ferrara, Ferrara, Italy

Abstract. – OBJECTIVE: A hernia of the abdominal wall is an opening of the muscles in the abdominal wall, which is frequently treated *via* the application of a surgical mesh. The purpose of this research is to study how human adipose-derived stem cells (hADSCs) interact with Phasix™ Mesh, a commercially available mesh for hernia repair. Studying how cells derived from the abdominal region behave with Phasix™ Mesh is crucial to improve the state of the art of current surgery and achieve effective tissue restoration.

MATERIALS AND METHODS: hADSCs were seeded onto Phasix™ Mesh, a fully resorbable surgical mesh of poly (4-hydroxybutyric acid) (P4HB). Cell viability was assessed through MTT assay, and cell growth and adhesion were evaluated *via* multiple imaging techniques and gene imaging profiling.

RESULTS: Results confirm that the nets support cells proliferation, extracellular matrix production and increasing of angiogenetic factor.

CONCLUSIONS: Butyric acid-based nets are promising scaffolds for abdominal wall reconstruction.

Key Words:
Abdominal wall hernia, Poly(4-hydroxybutyric acid) (P4HB), Phasix™ Mesh.

Introduction

A hernia of the abdominal wall is a weakness of the muscles in the abdominal wall that can lead to the protrusion of the abdominal content. More than 20 million hernia surgeries are performed on both adults and children every year worldwide[1,2]. Some of the main causes of hernias are obesity, other comorbidities, and surgery complications[1,3]. At present, hernia treatment consists in the implantation of a surgical mesh to close the defect and reinforce the damaged site[2,4,5].

In the context of regenerative medicine, tissue engineering is considered an encouraging option for the treatment of soft tissue damage[6,7]. Tissue engineering involves the use of biomaterials to repair and heal unfunctional or damaged tissues[8]. The ideal biomaterial should be biocompatible with the surrounding tissues, biodegradable to allow new tissue formation, non-toxic and non-immunogenic, and should have specific mechanical and morphological features to ensure the cells the appropriate microenvironment[9-11].

Biomaterials used in the abdominal wall hernia restoration aim at strengthening the anatomical site, conferring the tissue its mechanical features, and overall promoting tissue regeneration[12-14].

These biomaterials can be classified based on several properties – e.g., reabsorption ability, morphology, porosity, biological and chemical features[1,9,15-18], with different characteristics that make them suitable for any patient and type of surgery[1,19-21]. Meshes should close easily, be flexible, and ensure high wound strength[1,2,22,23]. Several biomaterials have been available for abdominal wall hernia repair: nylon and polyethylene terephthalate (PET) were the material of choice in the 1940s, nevertheless they have been widely replaced by polypropylene (PPL) since its discovery in 1954. Expanded polytetrafluoroethylene (ePTFE) and polyvinylidene fluoride (PVDF) are commercially available[1,2,24,25].

Corresponding Author: Barbara Zavan, MD; email: barbara.zavan@unife.it

Poly(4-hydroxybutyric acid) (P4HB) has been considered a valid material for surgical applications for over a decade, showing reduced infection and recurrence rates, as well as loose adhesion to the peritoneum[4,20,26]. P4HB is a synthetic absorbable polymer derived from a natural monomer that can be used as a monofilament mesh for the repair of damaged soft tissues; it degrades naturally through hydrolysis while providing long-term tensile strength in the application site[4]. Phasix™ Mesh is a surgical mesh consisting in a fully resorbable poly-4-hydroxybutyrate (P4HB) mesh combined with a hydrogel barrier[20,27,28]. Given its open-pore structure and the characteristics mentioned above, Phasix™ Mesh supports tissue ingrowth and vascularization resulting in rapid healing[29-32].

Mesenchymal stem cells hold specific biological features – notably, pluripotency, high replication rate, self-renewability, and low immunogenicity[33]. They are present in several body districts, including the adipose tissue, from whom they can be easily isolated via common surgical procedures – i.e., abdominoplasty or liposuction[34]. In this latter case they are specifically called human adipose-derived stem cells (hADSCs), and due to their regenerative properties, they can be considered a promising cell type for tissue engineering applications[17,33-37].

In this research we present an *in vitro* assessment of the interface of Phasix™ Mesh embedded with human adipose tissue-derived stem cells. We evaluated cell viability, adhesion and proliferation on the P4HB mesh by optical and electronical imaging analyses and gene expression profiling.

Materials and Methods

Cell Culture and Biomaterials

Human adipose-derived stem cells (hADSCs, Lonza Bioscience, Basel, Switzerland) were cultured in Dulbecco′s Modified Eagle′s Medium - high glucose (4500 mg/L glucose, L-glutamine, and sodium bicarbonate, without sodium pyruvate, liquid, sterile-filtered, Lonza Bioscience, Basel, Switzerland) supplemented with 2% Antibiotic Antimycotic Solution 100× (with 10.000 units penicillin, 10 mg streptomycin and 25 µg amphotericin B per mL, 0.1 µm filtered, Merck, Darmstadt, Germany) and 10% fetal bovine serum (16000044, GIBCO-Invitrogen, Waltham, MA, USA) at 37°C, and 5% CO_2.

The biomaterial used in this research is two commercially available surgical mesh, Phasix™ Mesh (BD, Franklin Lakes, NJ, USA) is a fully resorbable poly-4-hydroxybutyrate (P4HB) mesh combined with a hydrogel barrier[20,27,28]. Before seeding the cells, 0.5 × 0.5 cm squares of Phasix™ Mesh were cut and placed on a 24-well culture plate using sterile forceps.

MTT Assay

To determine cell viability in the Phasix™ Mesh, the MTT (3-4,5-dimethylthiazol-2yl-2,5-diphenyltetrazolium bromide)-based proliferation assay was performed. Briefly, the surgical mesh (0.5 × 0.5 cm) was incubated at 37°C for 3 h in 0.6 mL of 0.5 mg/mL MTT solution prepared in phosphate buffered saline (PBS, EuroClone, Milan, Italy). After removal of the MTT solution, 0.6 mL of 10% dimethyl sulfoxide in isopropanol was added to extract the formazan in the samples for 60 min at 37°C. For each sample, optical density values at 570 nm were recorded in duplicate on aliquots deposited in 96-well culture plates using a multilabel plate reader (PerkinElmer Wallac Victor2 1420 Multilabel Counter, Waltham, MA, USA).

RNA Extraction

Total RNA was isolated from cells grown on Phasix™ Mesh for 7 days using the total RNA purification Plus kit (Norgen Biotek, Toronto, ON, Canada). The RNA quality and concentration of the samples were measured with the NanoDrop™ ND-1000 (Thermo Fisher Scientific, Waltham, MA, USA). For one sample, 500 ng of total RNA was reverse transcribed using an RT2 First Strand kit (Qiagen, Hilden, Germany) in a final reaction volume of 20 µL. Sequencing of all RNAs was carried out by Area Science Park (ASP, Trieste, Italy) with Illumina sequencing.

SEM

Cellularized Phasix™ Mesh was fixed in 2% glutaraldehyde prepared in 0.1 M 4-(2-hydroxyethyl)-1-piperazineethanesulfonic acid (HEPES) buffer ON at +4°C. The mesh was then washed twice with 0.1 M HEPES buffer and progressively dehydrated by subsequent immersion in increasing concentrations of ethanol for 15 min each. The samples underwent chemical drying with hexamethyldisilane (Sigma-Aldrich, St. Louis, MO, USA), which was finally removed by complete evaporation before SEM imaging. The dry mesh was mounted on a specimen stub, and sputter-coated with gold alloy before examination in the microscope. All micrographs were obtained using a Zeiss EVO 40 SEM microscope (Zeiss, Jena, Germany) at Centro di Microscopia Elettronica (University of Ferrara, Ferrara, Italy).

Optical Microscopy and In Vitro Staining

The EVOS™ XL Core Imaging System (Thermo Fisher Scientific, Waltham, MA, USA) optical microscope equipped with 20x objective was used to acquire images of hADSCs growing on Phasix™ Mesh after 48 hours and 7 days of culture.

hADSCs on Phasix™ Mesh were fixed in 4% paraformaldehyde in PBS for 15 minutes, and then washed 3 times with PBS. Cells were stained with a Hoechst dye-blue, fluorescent stain solution for 15 minutes, protected from light. Eventually, cells were washed 2-3 times with PBS before proceeding with the imaging with Eclipse TE300 Inverted Microscope (Nikon Corporation, Minato, Tokyo, Japan) equipped with 20x and 40x objectives.

Library Preparation and RNA-Sequencing

The libraries were generated using 1 µg of total RNA by TruSeq Sample Preparation RNA Kit (Illumina, Inc., San Diego, CA, USA) according to the manufacturer's protocol without further modifications. cDNA libraries were checked on DNA 1000 Chip using Bioanalyzer 2100 (Agilent Technologies, Santa Clara, CA, USA) and quantified using Qubit™ dsDNA BR Assay Kit (Thermo Fisher Scientific, Waltham, MA, USA) on Qubit 2.0 Fluorometer (Thermo Fisher Scientific, Waltham, MA, USA). Sequencing was performed on Novaseq 6000 sequencer (Illumina, Inc., San Diego, CA, USA), generating for each sample almost 25 million of 2x150 bp paired-end reads. Illumina BCL2FASTQ v2.20 software was used for de-multiplexing and production of FASTQ sequence files. The resulting set of selected reads were aligned onto the complete human genome using Spliced Transcripts Alignment to a Reference algorithm STAR version 2.7.3. Mapping RNA-seq reads withSTAR. Curr. Protoc. Bioinformatics, 51, 11.14.1-11.14.19.] using hg38 Genome Assembly and Gencode.v35 as gene definition. The resulting Mapped reads were used as input for feature Counts function of Rsubread packages and used as Genes counts for Differentially expression analysis using Deseq2 package. Differentially expressed genes were selected if $|\log2(FC)| \leq$ or ≥ 1 and corrected p-value ≤ 0.05 and used as input to perform pathway enrichment analysis by IPA system (Ingenuity® Systems, www.ingenuity.com).

Statistical Analysis

For MTT assay analysis, the statistical methods included ANOVA test with multiple comparison between two groups: Phasix™ Mesh and the control condition. The one-way ANOVA test for comparative analysis of three or more groups using the GraphPad 8.0 software. Data were expressed as mean ± standard error of the mean (SE), and statistical significance was set at $p < 0.05$. RNA seq dataset was analyzed with QIAGEN Ingenuity Pathway Analysis software (QIAGEN, Hilden, Germany). Enrichment analysis and Venn diagram were performed with FunRich analysis tool. All experiments were conducted in triplicate.

Results

In Vitro Cell Viability and Proliferation

As shown in Figure 1, cell viability is improved in cells grown on Phasix™ Mesh for 48 hours, 7 days and 10 days, compared to the control group.

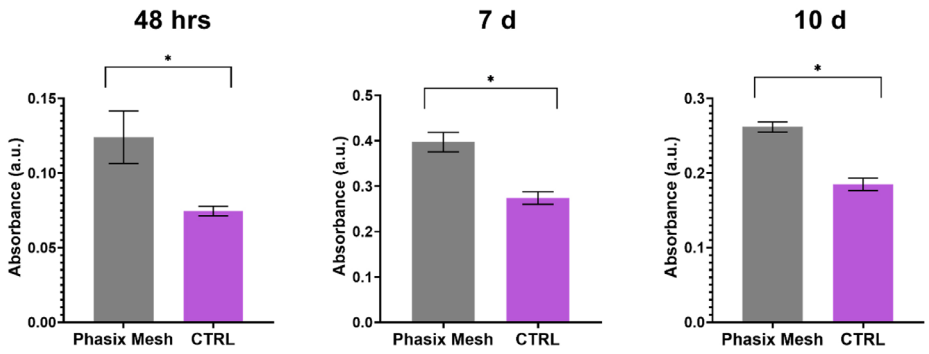

Figure 1. MTT assays absorbance values after 48 hours, 7 and 10 days of hADSCs grown onto Phasix™ Mesh and polystyrene (as control condition). Statistical significance is reported as * p<0,05.

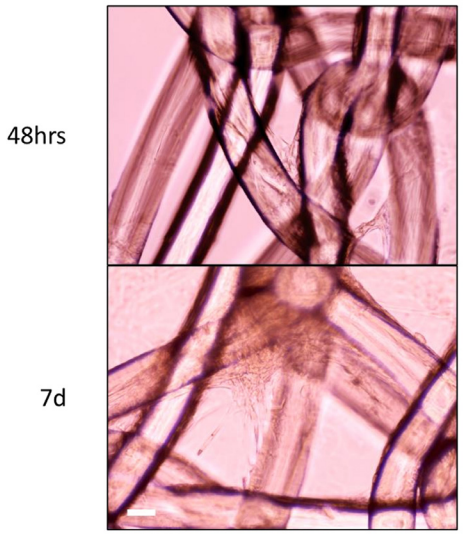

Figure 2. Optical microscope imaging of hADSCs grown onto Phasix™ Mesh. Images were taken at 48 hours and 7 days after seeding. Scale 200 µm.

At all timepoints, the difference in viability is statistically significant.

Cell proliferation on the mesh was monitored qualitatively by visualization though optical microscopy. Images in Figure 2 show the progression of cell colonization over time, after 2 and 7 days of culture. Cellular adhesion to the mesh can be observed in these images. Through fluorescence nuclear staining (Figure 3), we highlighted cellular growth between the mesh fibers: hADSCs grow in three-dimensional structures and fill Phasix™ Mesh via the production of extracellular matrix.

Visualization through SEM imaging also confirmed the presence of three-dimensional cell growth and cellular adhesion to the biomaterial (Figure 4).

RNA Sequencing

The dataset obtained from Ingenuity software analysis is comprised of 2217 differentially expressed gene (DEG) in cells grown on Phasix™ Mesh compared to the control, over a total of 15401 total entries. As represented in Figure 5 by the Volcano plot, hundreds of genes are upregulated (in red) or downregulated (in blue) in this dataset. Considering the DEGs with the highest fold change

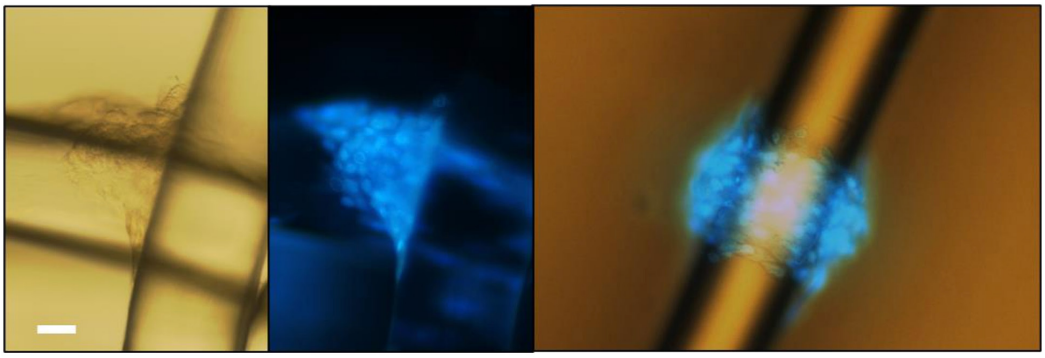

Figure 3. Fluorescence imaging of hADSCs nuclei (Hoeschst). Images were taken 7 days after cell culture on Phasix™ Mesh. Scale 100 µm.

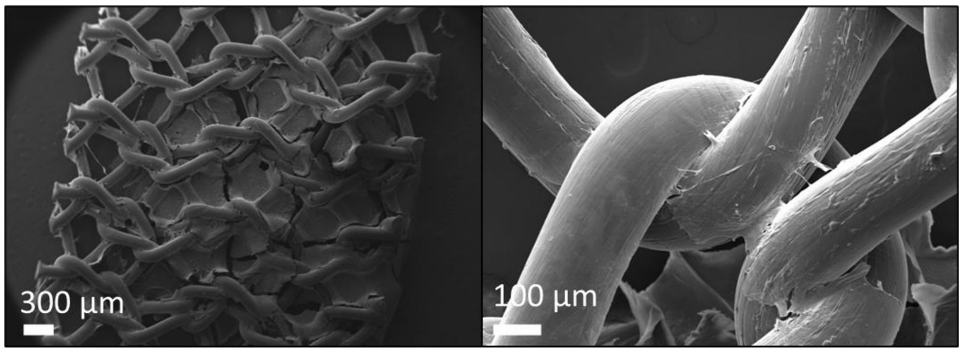

Figure 4. SEM imaging of hADSCs cells grown onto Phasix™ Mesh.

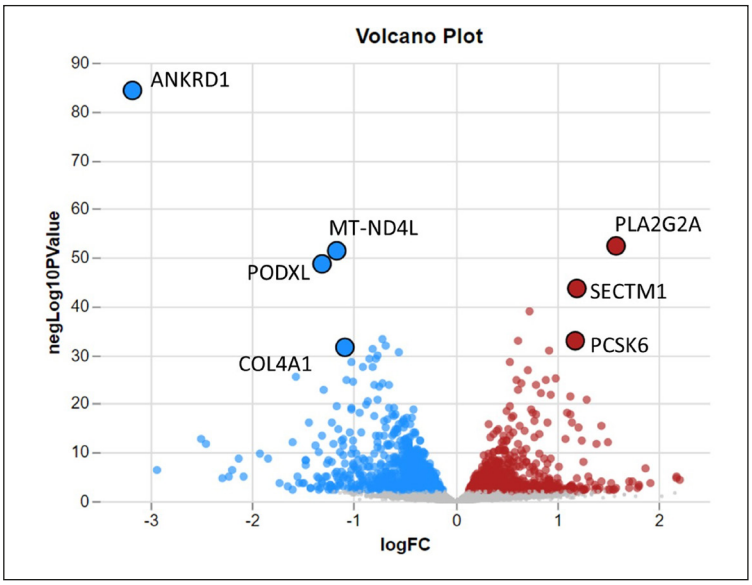

Figure 5. Volcano plot distribution of significantly differentially regulated genes in hADSCs grown on Phasix™ Mesh compared to hADSCs grown in control conditions. Up-regulated genes are in red, while downregulated genes are in blue. Non statistically relevant genes (p<0,5) are in grey. Most significant genes based on p-value and fold change are highlighted and labelled.

and the most significant p-value, the gene ANKRD1 (ENSG00000148677.7), encoding for ankyrin repeat domain 1, has the lowest expression ratio in Phasix™ group compared to the control.

ANKRD1 is followed by PODXL (ENSG00000128567.17), by MT-ND4L (ENSG00000212907.2), encoding for NADH dehydrogenase subunit 4L, and by collagen type IV alpha 1 chain's gene (COL4A1;

ENSG00000187498.16). Among the overexpressed genes, the most diverse expression is the one of PLA2G2A (ENSG00000188257.11), phospholipase A2 group IIA, SECTM1 (ENSG00000141574.8) and PCSK6 (ENSG00000140479.17).

Considering both fold change and p-value, DEGs were then categorized by the biological pathway in which they are involved, according to Ingenuity database (Table I). In the Phasix™ samples, thirteen DEGs are associated to three main pathways (to which a z-score has been attributed): Oxidative Phosphorylation (-3), Estrogen Receptor Signaling (-1.34) and Sirtuin Signaling Pathway (2.45). Oxidative Phosphorylation and Estrogen Receptor Signaling pathways are considered down-regulated, while Sirtuin Signaling is increased in Phasix™-grown sample (Table I). Figure 6A shows the expression ratio (in logarithmic scale) for each of the 13 genes involved in these pathways (MT-

Table I. Canonical Pathways identified by Ingenuity software listed in order of statistical relevance (p-value). Z-Score is also reported for each pathway as a measure of confidence of the prediction: activated (>2) or deactivated (<2). The Molecules involved in each pathway are listed in the last row.

	Ingenuity Canonical Pathways	-log (p-value)	z-score	Molecules
Phasix™ Mesh	Oxidative Phosphorylation	10,4	-3	MT-ATP6,MT-CO1,MT-CO3,MT-CYB,MT-ND1,MT-ND2,MT-ND4,MT-ND4L,MT-ND5
Vs	Estrogen Receptor Signaling	7,47	-1,341640786	MT-ATP6,MT-CYB,MT-ND1,MT-ND2,MT-ND4,MT-ND4L,MT-ND5,MT-ND6,PGR,TRIM63
CTRL	Sirtuin Signaling Pathway	5,59	2,449489743	MT-ATP6,MT-CYB,MT-ND1,MT-ND2,MT-ND4,MT-ND4L,MT-ND5,MT-ND6

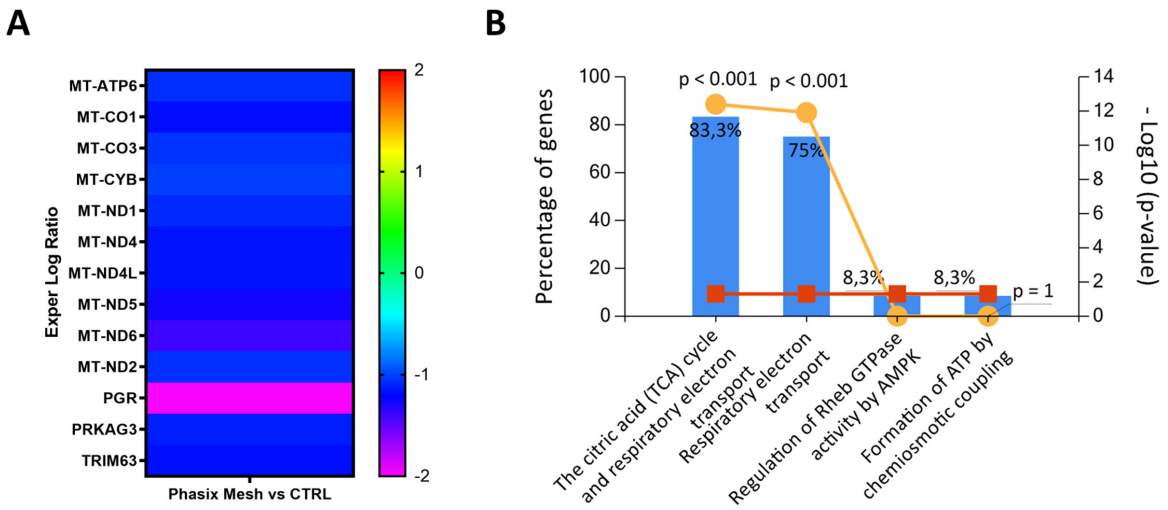

Figure 6. **A,** Heatmap of DEGs involved in Oxidative Phosphorylation, Estrogen Receptor Signaling and Sirtuin Signaling Pathway. Gene expression in expressed in logarithmic ratio of Phasix Mesh condition over control conditions. **B,** Distribution of DEGs of interest regarding their role in biological pathways (result of FunRich enrichment analysis).

ATP6, MT-CO1, MT-CO3, MT-CYB, MT-ND1, MT-ND2, MT-ND4, MT-ND4L, MT-ND5, MT-ND6, PGR, PRKAG3 and TRIM63). All the DEG are downregulated by 1 to 2 folds in Phasix™ samples. Further analysis of these genes' function with FunRich software underlined that 83.3% of them are involved in the citric acid cycles, 75% are involved more broadly in the respiratory electron transport chain Figure 6B.

According to Ingenuity software, the downregulation of the above-mentioned DEG and related canonical pathways ultimately indicates a decrease in Neutrophile Activation, with an attributed z-scores of -2,596 (Table II). In the Volcano plot representation (Figure 7A), all genes involved in the Activation of neutrophiles pathway are represented. The plot shows six mitochondrial genes (MT-ND4L, MT-ND5, MT-ND6, MT-CO1, MT-CYB, MT-ND4) heavily and significantly downregulated, while PLA2GA2A is upregulated. In Table II other statistically relevant functions concerning the Phasix™ sample are also mentioned, for which Ingenuity has made a confident activation state prediction: Activation

Table II. Functions identified by Ingenuity software listed in order of statistical relevance (*p*-value). Z-Score is also reported for each pathway as a measure of confidence of the prediction: activated (>2) or deactivated (<2). The Molecules involved in each pathway are listed in the last row.

	Diseases or Functions Annotation	*p*-value	Predicted Activation State	Activation z-score	Molecules
Phasix™	Activation of neutro phils	1.56 E-09	Decreased	-2,596	MT-CO1,MT-CYB,MT-ND2,MT-ND4,MT-ND4L,MT-ND5,MT-ND6,PLA2G2A
Mesh Vs	Activation of cells	0.00 033	Decreased	-2,563	CD24,ITGAX,MT-CO1,MT-CYB,MT-ND2,MT-ND4,MT-ND4L,MT-ND5,MT-ND6,PLA2G2A,PMEL,RGCC, SPRY1,TRH
CTR L	Activation of leukocytes	0.00 0458	Decreased	-2,532	CD24,MT-CO1,MT-CYB,MT-ND2,MT-ND4,MT-ND4L,MT-ND5,MT-ND6,PLA2G2A,PMEL,SPRY1

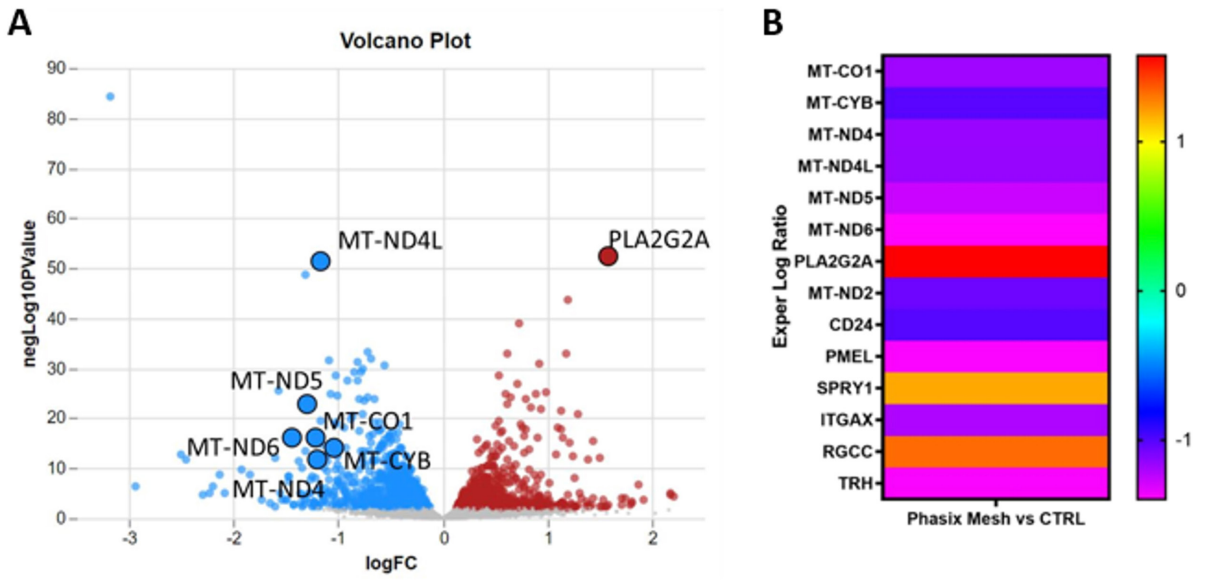

Figure 7. A, Volcano plot distribution of significantly differentially regulated genes in hADSCs grown on Phasix^{TM} Mesh compared to hADSCs grown in control conditions. Upregulated genes are in red, while downregulated genes are in blue. Non statistically relevant genes (p<0.5) are in grey. Labels show genes involved in Activation of Neutrophils pathway. **B,** Heatmap of DEGs involved in Activation of neutrophils, Activation of cells and Activation of leukocytes. Gene expression in expressed in logarithmic ratio of Phasix^{TM} Mesh condition over control conditions.

of cells (Z-score -2.563) and Activation of leukocytes (z-score -2.532). Of all fourteen DEGs involved in these pathways (MT-CO1, MT-CYB, MT-ND4, MT-NDL4, MT-ND5, MT-ND6, PLA2G2A2, MT-ND2, CD24, PMEL, SPRY1, ITGAX, RGCC, THR), eight of them are involved in all three functions, while three are involved in the activation of cells and leukocytes and three others are involved in cell activation only (Figure 8). Figure 7A shows the fold change for each gene: only PLA2G2A, SPRY1 and RGCC are overexpressed in the Phasix™ Mesh compared to the control.

The output dataset from Ingenuity software also contained several DEGs involved in extracellular matrix production, although they were not associated with any specific biological pathway. In Figure 9 is reported the expression rate of all collagen

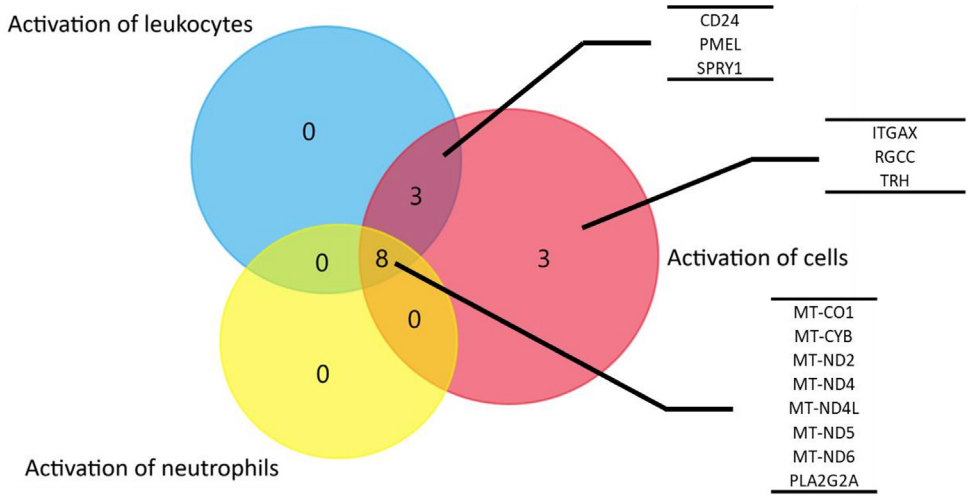

Figure 8. Venn Diagram of DEGs distribution in Activation of neutrophils, Activation of Cells and Activation of leukocytes pathways.

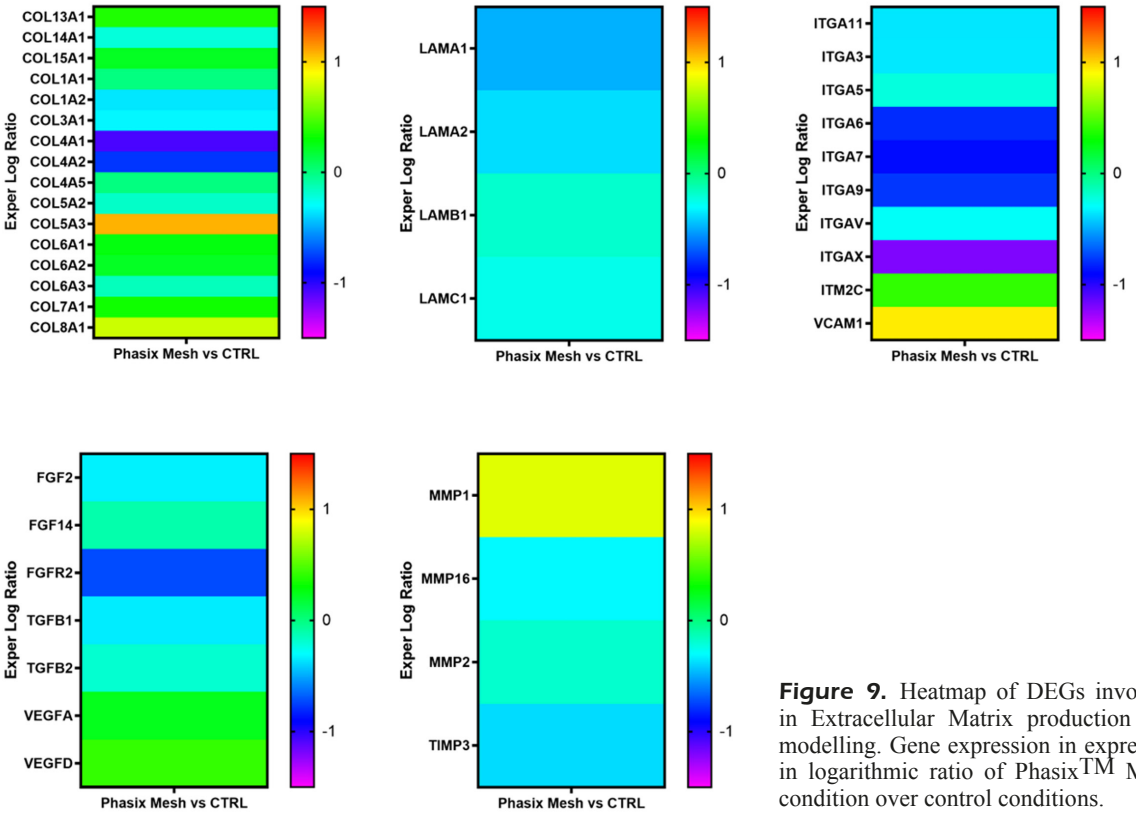

Figure 9. Heatmap of DEGs involved in Extracellular Matrix production and modelling. Gene expression in expressed in logarithmic ratio of Phasix^{TM} Mesh condition over control conditions.

chain types present in the dataset: COL5A3, COL6A1, COL6A2, COL7A1, COL8A2, COL13A1 and COL15A1 are overexpressed in Phasix™ Mesh samples, while COL1A1, COL1A2, COL3A1, COL4A2, COL4A5, COL5A2, COL6A3, COL6A6 and COL14A1 are downregulated. Genes encoding for laminin chains LAMA1, LAMA2, LAMA3, LAMA5, LAMB1 and LAMC1 are also downregulated (Figure 9). Concerning adhesion proteins, genes ITGA3, ITGA5, ITGA6, ITGA7, ITGA9, ITGA11, ITGAV and ITGAX are all under expressed, while Vascular cell adhesion molecule (VCAM) is overexpressed in Phasix™ samples (Figure 9). Regarding growth factors, we found that Fibroblast Growth Factor 2 (FGF2) and FGF receptor 2 (FGFR2) were both downregulated in Phasix™ compared to the control, and so is TGF-Beta-1 and 2. On the other hand, Vascular Endothelial Growth Factor A and D (VEGFA and VEGFD) expression in increased (Figure 9).

Beside TGFB, in the dataset we found other genes involved in the Inflammation Response (Figure 10). Of these, Interleukins 33 and 36 are less expressed in Phasix™ samples, while Prostaglandin-Endoperoxide Synthase 2 (PTGS2) and (Beta-2-Microglobulin) B2M are upregulated.

Discussion

Abdominal wall defects can be derived from by infection, trauma, and tumor resection. Due to the complexity of the defects, its reconstruction remains a surgical challenge. In this context, tissue engineering based on biomaterials as scaffolds to guide tissue regeneration offers to the surgery a promising approach for the reconstruction of abdominal wall defects. Great attention must be reserved to their properties since they should do hernia, chronic pain or infection. In this work we tested in vitro butyric acid-based nets, confirming that no immunological response is present, and that they show a great ability to promote cell proliferation and the regeneration of extracellular matrix important to improve the reconstruction and to enhance resistance to contamination and infection. Moreover, our results confirm the activation of special intracellular pathways such as Sirtuin Signaling, reduction on redox related metabolism, increasing cells adhesion proteins and Vascular cell adhesion molecule such as VCAM or other vascular regenerative factors such as Vascular Endothelial Growth Factor A and D (VEGFA and VEGFD).

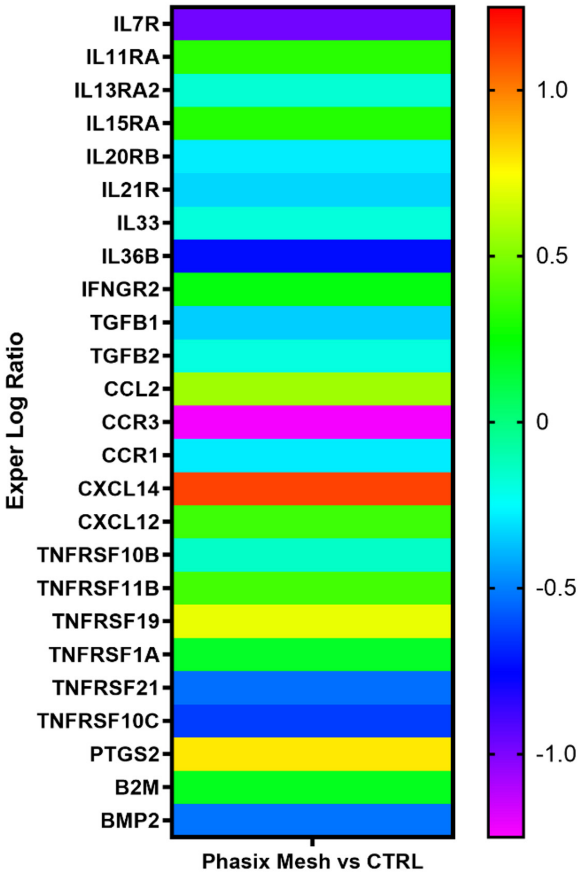

Figure 10. Heatmap of DEGs involved in Inflammation Response pathways. Gene expression in expressed in logarithmic ratio of Phasix^{TM} Mesh condition over control conditions.

Conclusions

In light of such results, we can confirm that butyric acid-based scaffolds are promising biomaterials to support abdominal wall reconstruction.

Authors' Contributions

Conceptualization, B.Z.; methodology, E.T., F.Z.; software, M.T.; validation, M.T., F.Z.; formal analysis, M.T., F.Z., E.T., I.Z.; investigation, I.Z., M.T., F.Z., E.T.; resources, M.T., I.Z.; data curation, M.T.; writing—original draft preparation, I.Z., M.T., E.T., F.Z., B.Z.; writing—review and editing, I.Z., M.T., E.T., F.Z., B.Z.; supervision, G.S; B.Z.; project administration, C.M; B.Z.; funding acquisition, B.Z. All authors have read and agreed to the published version of the manuscript.

ORCID

Ilaria Zanolla: https://orcid.org/0000-0002-7395-787X
Elena Tiengo: https://orcid.org/0000-0003-4610-2339
Federica Zanotti: https://orcid.org/0000-0002-8721-8162
Martina Trentini: https://orcid.org/0000-0001-9243-6466
Carmen Mortellaro: https://orcid.org/0000-0002-1150-1906
Danilo Licastro: https://orcid.org/0000-0001-8372-9355
Simeone Dal Monego: https://orcid.org/0000-0002-2285-2461
Barbara Zavan: https://orcid.org/my-orcid?orcid=0000-0002-4779-4456

Conflict of Interest

The Authors declare that they have no conflict of interests.

Data Availability Statement

The datasets generated during and/or analyzed during the current study are available from the corresponding author on reasonable request.

Ethics Committee approval and Informed Consent

Not applicable.

References

1) Serrano-Aroca Á, Pous-Serrano S. Prosthetic meshes for hernia repair: State of art, classification, biomaterials, antimicrobial approaches, and fabrication methods. J Biomed Mater Res A 2021; 2695-2719.
2) Liu Z, Wei N, Tang R. Functionalized Strategies and Mechanisms of the Emerging Mesh for Abdominal Wall Repair and Regeneration. ACS Biomater Sci Eng 2021; 2064-2082.
3) Tran H. Endorsement of the HerniaSurge guidelines by the Australasian Hernia Society. Hernia 2018; 177.
4) Levy AS, Bernstein JL, Premaratne ID, Rohde CH, Otterburn DM, Morrison KA, Lieberman M, Pomp A, Spector JA. Poly-4-hydroxybutyrate (PhasixTM) mesh onlay in complex abdominal wall repair. Surg Endosc 2021; 35: 2049-2058.
5) Butler CE, Baumann DP, Janis JE, Rosen MJ. Abdominal wall reconstruction. Curr Probl Surg 2013; 50: 557-586.
6) Azzena B, Mazzoleni F, Abatangelo G, Zavan B, Vindigni V. Autologous platelet-rich plasma as an adipocyte in vivo delivery system: Case report. Aesthetic Plast Surg 2008; 32: 155-158.
7) Kalaba S, Gerhard E, Winder JS, Pauli EM, Haluck RS, Yang J. Design strategies and applications of biomaterials and devices for Hernia repair. Bioact Mater 2016; 2-17.
8) Brun P, Cortivo R, Zavan B, Vecchiato N, Abatangelo G. In vitro reconstructed tissues on hyaluronan-based temporary scaffolding. J Mater Sci Mater Med 1999; 10: 683-688.
9) Figallo E, Flaibani M, Zavan B, Abatangelo G, Elvassore N. Micropatterned biopolymer 3D scaffold for static and dynamic culture of human fibroblasts. Biotechnol Prog 2007; 210-216.

10) Ferroni L, Gardin C, Sivolella S, Brunello G, Berengo M, Piattelli A, Bressan E, Zavan B. A hyaluronan-based scaffold for the in vitro construction of dental pulp-like tissue. Int J Mol Sci 2015; 16: 4666-4681.

11) Bressan E, Favero V, Gardin C, Ferroni L, Iacobellis L, Favero L, Vindigni V, Berengo M, Sivolella S, Zavan B. Biopolymers for Hard and Soft Engineered Tissues: Application in Odontoiatric and Plastic Surgery Field. Polymers 2011; 509-526.

12) Lee EJ, Kasper FK, Mikos AG. Biomaterials for tissue engineering. Ann Biomed Eng 2014; 323-337.

13) Sharma K, Mujawar MA, Kaushik A. State-of-Art Functional Biomaterials for Tissue Engineering. Front Mater 2019; 6.

14) Berthiaume F, Maguire TJ, Yarmush ML. Tissue engineering and regenerative medicine: History, progress, and challenges. Annu Rev Chem Biomol Eng 2011; 403-430.

15) Brown CN, Finch JG. Which mesh for hernia repair? Ann R Coll Surg Engl 2010; 272-278.

16) Deeken CR, Lake SP. Mechanical properties of the abdominal wall and biomaterials utilized for hernia repair. J Mech Behav Biomed Mater 2017; 411-427.

17) Gardin C, Bressan E, Ferroni L, Nalesso E, Vindigni V, Stellini E, Pinton P, Sivolella S, Zavan B. In vitro concurrent endothelial and osteogenic commitment of adipose-derived stem cells and their genomical analyses through comparative genomic hybridization array: Novel strategies to increase the successful engraftment of tissue-engineered bone grafts. Stem Cells Dev 2012; 21: 767-777.

18) Todros S, Pavan PG, Pachera P, Natali AN. Synthetic surgical meshes used in abdominal wall surgery: Part II—Biomechanical aspects. J Biomed Mater Res B Appl Biomater 2017; 892-903.

19) Chowbey P, Lomanto D. Techniques of abdominal wall hernia repair. Springer, 2020.

20) Gómez-Gil V, Pascual G, Bellón JM. Biomaterial implants in abdominal wall Hernia Repair: A review on the importance of the peritoneal interface. Processes 2019; 7: 105.

21) Amid PK. Classification of biomaterials and their related complications in abdominal wall hernia surgery. Hernia. Springer-Verlag 1997; 1: 15-21.

22) Vrijland WW, Jeekel J, Steyerberg EW, den Hoed PT, Bonjer HJ. Intraperitoneal polypropylene mesh repair of incisional hernia is not associated with enterocutaneous fistula. Br J Surg 2000; 87: 348-352.

23) Klinge U, Klosterhalfen B. Modified classification of surgical meshes for hernia repair based on the analyses of 1,000 explanted meshes. Hernia 2012; 16: 251-258.

24) Greco DP, Abbati C. Biomaterials in Abdominal Wall Surgery. Springer International Publishing 2019; 51-61.

25) Coda A, Lamberti R, Martorana S. Classification of prosthetics used in hernia repair based on weight and biomaterial. Hernia 2012; 9-20.

26) Utsunomia C, Ren Q, Zinn M. Poly(4-Hydroxybutyrate): Current State and Perspectives. Front Bioeng Biotechnol. 2020; 8: 257.

27) Deeken CR, Faucher KM, Matthews BD. A review of the composition, characteristics, and effectiveness of barrier mesh prostheses utilized for laparoscopic ventral hernia repair. Surg. Endosc 2012; 26: 566-575.

28) Deeken CR, Lake SP. Mechanical properties of the abdominal wall and biomaterials utilized for hernia repair. J Mech Behav Biomed Mater 2017; 411-427.

29) Yu D, Patel AT, Rossi K, Topham NS, Chang EI. Comparison of Phasix™, polypropylene, and primary closure of the abdominal donor site after bilateral free flap breast reconstruction: Long-term evaluation of abdominal hernia and bulge formation. Microsurgery 2020; 40: 434-439.

30) Affolter M, Zeller R, Caussinus E. Tissue remodelling through branching morphogenesis. Nat Rev Mol Cell Biol 2009; 831-842.

31) Gómez-Gil V, Rodríguez M, García-Moreno Nisa F, Pérez-Köhler B, Pascual G. Evaluation of synthetic reticular hybrid meshes designed for intraperitoneal abdominal wall repair: Preclinical and in vitro behavior. PLoS ONE 2019; 14.

32) Martin DP, Badhwar A, Shah DV, Rizk S, Eldridge SN, Gagne DH, Ganatra A, Darois RE, Williams SF, Tai HC, Scott JR. Characterization of poly-4-hydroxybutyrate mesh for hernia repair applications. J Surg Res 2013; 184: 766-773.

33) Zavan B, Giorgi C, Bagnara GP, Vindigni V, Abatangelo G, Cortivo R. Osteogenic and chondrogenic differentiation: comparison of human andrat bone marrow mesenchymal stem cells cultured into polymeric scaffolds. Eur J Histochem 2007; 51: 1-8.

34) Zavan B, Michelotto L, Lancerotto L, della Puppa A, D'Avella D, Abatangelo G, Vindigni V, Cortivo R. Neural potential of a stem cell population in the adipose and cutaneous tissues. Neurol Res 2010; 32: 47-54.

35) Han YF, Tao R, Sun TJ, Chai JK, Xu G, Liu J. Advances and opportunities for stem cell research in skin tissue engineering. Eur Rev Med Pharmacol Sci 2012; 16: 1873-1877.

36) Annibali S, Cristalli MP, Tonoli F, Polimeni A. Stem cells derived from human exfoliated deciduous teeth: a narrative synthesis of literature. Eur Rev Med Pharmacol Sci 2014; 18: 2863-2881.

37) Brasset C, Allemann P, Sauvain MO. Recurrent complex incisional hernia repair by enhanced-view totally extraperitoneal (eTEP) technique. Eur Rev Med Pharmacol Sci 2021; 25: 5452-5457.